Polymer Chemistry

ROYAL SOCIETY OF CHEMISTRY

PAPER

View Article Online
View Journal | View Issue

Cite this: *Polym. Chem.*, 2022, **13**, 5135

The effect of surface-active statistical copolymers in low-energy miniemulsion and RAFT polymerization†

Manon Rolland, [a] Eric R. Dufresne, [b] Nghia P. Truong *[a,c] and Athina Anastasaki *[a]

Low-energy miniemulsions enable the production of uniform nanodroplets for a wide range of applications without the need for using specialized equipment. However, low-energy miniemulsions are typically formed in the presence of a surface-active agent with a specific structure and property. In this work, we elucidate the role of a surface-active statistical copolymer, poly(*N*-(2-hydroxypropyl) methacrylamide-*co*-di(ethylene glycol) ethyl ether methacrylate) P(HPMA-*co*-DEGMA), in the formation of low-energy miniemulsions and reversible addition–fragmentation chain-transfer (RAFT) polymerization, enabling the design of a new series of surface-active statistical copolymers. In particular, we found that the HPMA/DEGMA ratio and copolymer molecular weight significantly affect the interfacial tension between water and styrene and as a result, the size of nanodroplets and the RAFT miniemulsion polymerization. Importantly, these findings allowed for the design and synthesis of novel surface-active statistical copolymers composed of DEGMA and various hydrophilic moieties that can also substantially lower the interfacial tension to below 12 mN m^{-1}. Furthermore, the new copolymer of DEGMA with methacrylamide (MAAm) resulted in the smallest nanodroplet size. This copolymer was subsequently selected to trigger the RAFT polymerization of styrene yielding nanoparticles of different morphologies including worm balls, worms, and vesicles. This work sheds light on the role of surface-active statistical copolymers and significantly expands the availability of surface-active agents for low-energy miniemulsion and RAFT polymerization.

Received 12th April 2022,
Accepted 18th August 2022

DOI: 10.1039/d2py00468b

rsc.li/polymers

Introduction

Miniemulsions, also referred to as nanoemulsions, are kinetically stable dispersions of oil droplets in water (typically ranging between 20–500 nm)[1–3] and have found use in numerous applications ranging from drug delivery and cosmetics to food industry and polymer synthesis.[4–7] The combination of miniemulsions with controlled radical polymerizations is particularly attractive due to the higher polymerization rates and minimized termination observed when compared to traditional solution polymerizations.[8–13] Another unique property of an ideal miniemulsion polymerization is the so-called 1 : 1 copy feature whereby each monomer nanodroplet is transformed to one polymeric nanoparticle of a similar size.[14–17] Miniemulsions require high energy input to trigger their formation.[18,19] Therefore, the vast majority of reported methods necessitate high mechanical force to effectively disperse the oily monomers in water which may be problematic due to possible degradation of shear- and/or heat-sensitive monomers.[5,10,12,20–22] Furthermore, high energy methods often require the use of costly and specialized equipment (*e.g.* high-pressure homogenizers, high-shear stirrers or sonication) which may not only be unavailable to many laboratories but also pose a high risk of metal contamination prohibiting the widespread use of miniemulsion technology.[19] To overcome these issues, low-energy methods have been developed including phase inversion composition, phase inversion temperature, membrane emulsification, *in situ* surfactant formation, bubble-bursting and spontaneous method.[23–30] It is noted that low-energy miniemulsions are rarely combined with controlled-radical polymerization strategies.[13,31–33] Undoubtedly, Zetterlund and co-workers pioneered the field by reporting a

[a]*Laboratory of Polymeric Materials, Department of Materials, ETH Zürich, Vladimir-Prelog-Weg 5, 8093 Zürich, Switzerland. E-mail: athina.anastasaki@mat.ethz.ch, nghia.truong@monash.edu*
[b]*Laboratory of Soft and Living Materials, Department of Materials, ETH Zürich, Vladimir-Prelog-Weg 5, 8093 Zürich, Switzerland*
[c]*Monash Institute of Pharmaceutical Sciences, Monash University, 399 Royal Parade, Parkville, VIC 3152, Australia*

†Electronic supplementary information (ESI) available: Material, instrumentation and procedures. See DOI: https://doi.org/10.1039/d2py00468b

low-energy emulsification method that involved the gradual dilution of a microemulsion precursor to form styrene nanodroplets with excellent particle size stability throughout the polymerization.[34] The same group subsequently developed an *in situ* surfactant low-energy method whereby oleic acid and potassium hydroxide spontaneously reacted at the interface and in the absence of high energy mixing. The miniemulsion formed was then heated to 70 °C and a RAFT polymerization of styrene took place.[35] In another contribution, Zetterlund's group exploited the use of low-pressure CO_2 and by modulating the pressure range, the formation of miniemulsion could be obtained.[36] Our group has also recently reported a low-energy miniemulsion method to produce nanoparticles with different morphologies by utilizing a special statistical copolymer, namely poly(*N*-(2-hydroxypropyl) methacrylamide-*co*-di (ethylene glycol) ethyl ether methacrylate)) P(HPMA-*co*-DEGMA) which decreased the interfacial tension between monomer and water.[37] Importantly, our approach operated by simple handshaking and in the absence of any external deoxygenation while styrenic, methacrylic and acrylic diblock copolymers could successfully be produced. After the polymerization was completed and through a morphological transformation strategy,[38] different morphologies could be obtained including spheres, worms, and vesicles. However, low-energy miniemulsion methods often require a specific surface-active agent such as P(HPMA-*co*-DEGMA) to reduce the surface tension and their detailed structure/property relationship has been rarely studied. In this work, we aim to understand the role of surface-active P(HPMA-*co*-DEGMA) and expand the scope of our recently reported system by employing various new surface-active copolymers. First, the effect of the HPMA/DEGMA ratio within the statistical copolymer composition was investigated. The molecular weight of the copolymer was also assessed. To expand the availability of surface-active copolymers and provide a more inexpensive alternative than HPMA, various statistical copolymers were also synthesized and their role as efficient surfactants and macromolecular chain transfer agents (macro-CTAs) was explored (Fig. 1). The most promising statistical copolymer was subsequently used to prepare nanoparticles of different shapes, thus providing a less costly surface-active alternative.

Results and discussion

Low-energy miniemulsion with variable P(HPMA-*co*-DEGMA) composition

To form the low-energy miniemulsion, an oily monomer (*i.e.* styrene, 35 μL, 1.2 wt% relative to water), water (2 mL), a small molecule surfactant, namely sodium dodecyl sulfate (SDS) (0.25 mg, 0.8 wt% relative to styrene), and a macromolecular chain transfer agent (25 mg, 78 wt% relative to styrene) were mixed at room temperature by simple handshaking for approximately 10 seconds (Fig. 1).[37] P(HPMA-*co*-DEGMA) was

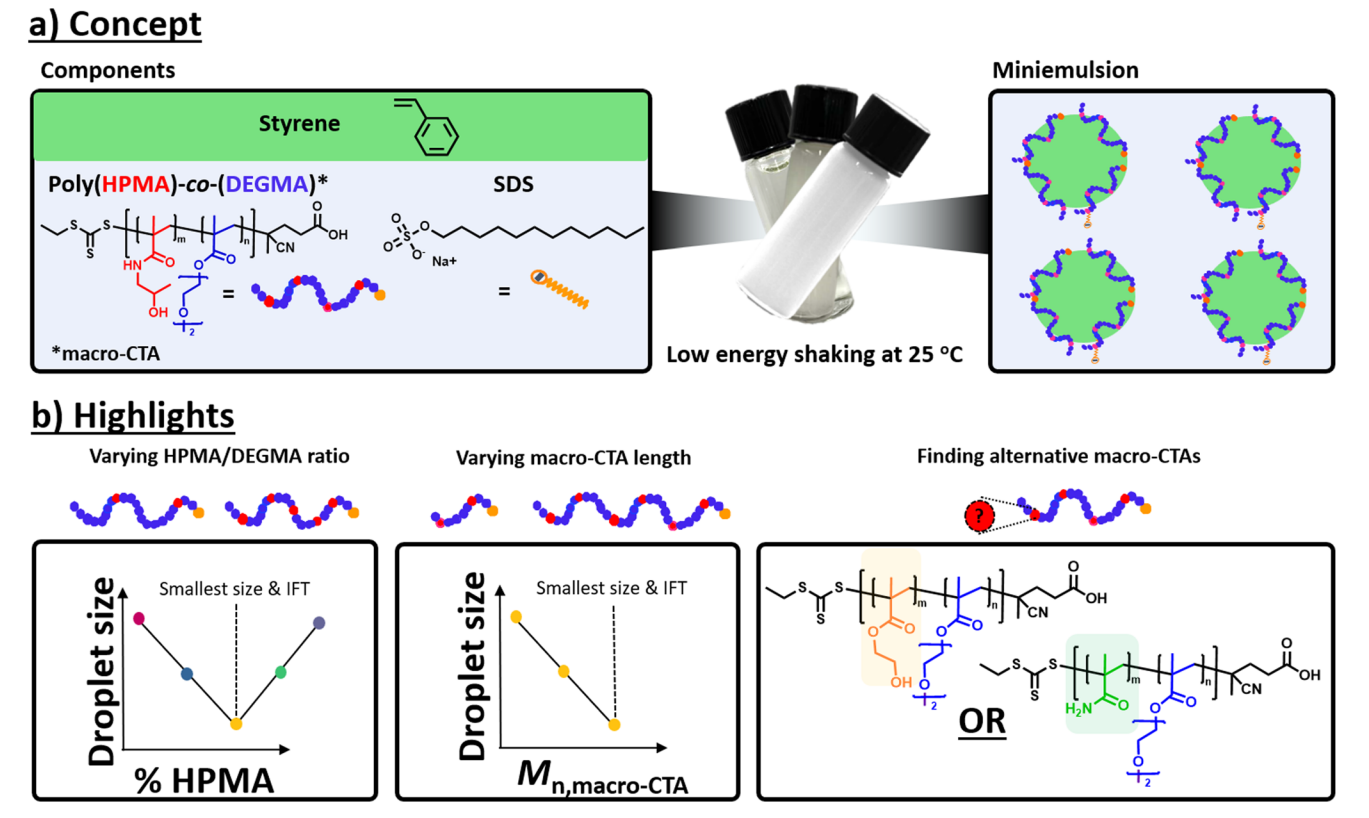

Fig. 1 Schematic representation of (a) low-energy miniemulsion formation at room temperature and (b) highlights of our current study.

first employed as a surface-active copolymer as well as a macro-CTA for the formation of miniemulsion and RAFT polymerization. In our previous work, we synthesized a macro-CTA with ~20% HPMA content whereby the length of DEGMA was fixed at 31 units while the length of HPMA was set to 7 units.[37] This formulation led to the formation of nanodroplets with a diameter of ~180 nm, as characterized by dynamic light scattering (DLS). It is noted that the nanodroplets were only obtained in the presence of SDS, otherwise rapidly coalescing into larger aggregates.[37] However, the impact of the copolymer composition on the interfacial tension between water and oil and as a result, the formation of the nanodroplets remains unclear.

To investigate this, a series of copolymers were prepared with variable HPMA compositions. In particular, a library of random copolymers was synthesized by RAFT solution polymerizations in which the DEGMA content was kept constant at ~31 units while the HPMA composition was gradually increased from 3 units (macro-CTA A1) to 8 (macro-CTA A2), 13 (macro-CTA A3) and 24 (macro-CTA A4), corresponding to 10, 20, 30 and 43% of HPMA respectively. A poly(DEGMA) homopolymer (0% HPMA content) was also synthesized (macro-CTA A0) and all macro-CTAs were thoroughly characterized by nuclear magnetic resonance (NMR) and size exclusion chromatography (SEC) to determine their precise composition and molecular characteristics respectively (Fig. 2a, S1 and

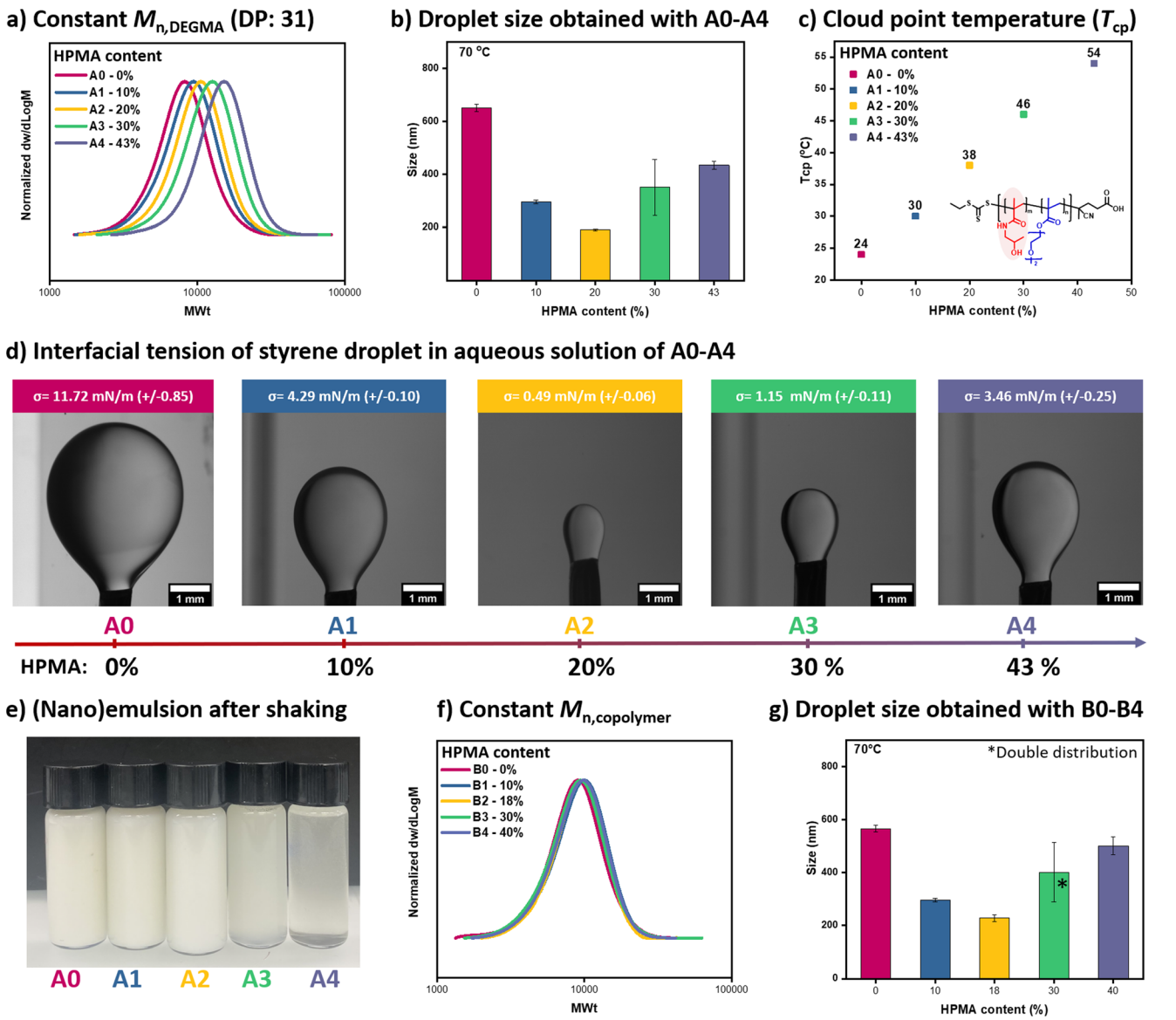

Fig. 2 (a) SEC traces of macro-CTAs A0–A4, (b) DLS sizes (by number at 70 °C) of (mini)emulsion formed by using A0–A4 with the following formulation: [macro-CTA] : [STY] : [SDS] = 25 mg : 35 μL : 0.25 mg, in 2 mL of deionized water (mass constant), (c) cloud point temperature of A0–A4, (d) interfacial tension of styrene droplet in an aqueous solution of macro-CTAs (A0–A4) measured by inverse pendant drop method, (e) pictures of (mini)emulsion formed by using A0–A4, (f) SEC traces of macro-CTAs B0–B4 and (g) DLS sizes (by number at 70 °C) of (mini)emulsion formed with B0–B4 with the following formulation: [macro-CTA] : [STY] : [SDS] = 1 (25 mg): 97 (35 μL) : 0.3 (0. 25 mg), in 2 mL of deonized water.

Table S1†). All macro-CTA are water-soluble at room temperature and the concentration of SDS used is well below its CMC, thus precluding the formation of initial micelles/aggregates (Fig. S2†). The mixtures of each macro-CTA together with styrene, SDS, and water were then shaken for approximately 10 seconds and the results are summarized in Fig. 2 & S3 ([macro-CTA] : [STY] : [SDS] = 25 mg : 35 μL : 0.25 mg, in 2 mL of water). Upon increasing the HPMA content from 0 to 10 and 20% (macro-CTAs A0, A1, and A2), the nanodroplet size gradually decreased from 642 to 321 and 180 nm respectively (Fig. 2b, S3 and Table S2†). Notably, these miniemulsions are thermodynamically unstable as they phase separate with time (>2 days, Fig. S4†). Also, a similar size could be obtained at both room temperature and 70 °C due to the presence of SDS that stabilize the nanodroplets by electrostatic repulsion (Fig. 2b, S3 and Table S2†).

To understand the variation in the diameter of the nanodroplets, we subsequently conducted pendant drop tensiometry measurements.[39] A0 showed an interfacial tension of 11.7 mN m^{-1} while A1 and A2 displayed interfacial tension values of 4.4 mN m^{-1} and 0.5 mN m^{-1} respectively. It is therefore apparent that increasing the HPMA content (from 0% to 20%) leads to lower interfacial tension and smaller size of the observed nanodroplets (Fig. 2a–d, and Tables S1–2†). However, this trend was reversed when the HPMA content was increased further (from 20% to 43%). The data suggest that the hydrophilicity balance of the copolymer is an important parameter affecting the interfacial tension and the droplet size. For small-molecule surfactants, it is known that the hydrophilic–lipophilic balance (HLB) also plays an important role in the formation of miniemulsions.[40–42] Without the hydrophilic segment HPMA, PDEGMA (macro-CTA A0) partitioned mostly in the styrene phase while when HPMA was incorporated (macro-CTAs A1 and A2), the copolymer became more surface-active. However, when the copolymer contains more HPMA (macro-CTAs A3 and A4), it might be more present in the water phase (than in the styrene phase or on the droplet surface) as the interfacial tension was reduced less. The partitioning of these macro-CTAs between the two phases was examined through simple solubility experiments.[43] Macro-CTAs A0 presented very high solubility in styrene owing to its relatively hydrophobic nature (Fig. S5 and Table S3†). This is also in agreement with the cloud point temperatures (T_{cp}) of this macro-CTA which is 24 °C (Table S1†). Below this temperature, A0 is water-soluble but when increasing the temperature to above the T_{cp} the A0 solution becomes cloudy. When 10% and 20% of HPMA were incorporated (A1 and A2 macro-CTA) the T_{cp} was increased to 30 and 38 °C, respectively (Fig. 2c and Table S1†). This data highlight that when particularly high affinity with the hydrophobic phase (*i.e.* styrene) is observed, higher interfacial tensions and larger size are obtained (Fig. 2, S3 & S5, Tables S1 & S3†). In contrast, A2 presented a comparable solubility in both styrene and water (requiring roughly 2 minutes to be fully dissolved in either media) and this led to the minimum interfacial tension and smallest size obtained (Fig. 2, S3 & S5, Tables S1–3†). The same rationale can be followed to understand the data acquired when the more hydrophilic A3 and A4 macro-CTAs were employed. The increase in the HPMA composition led to an overall increase in the macro-CTA's hydrophilicity leading to a further increase in the T_{cp} (46 and 54 °C, Fig. 2c, and Table S1†). This was visually evident by the enhanced solubility of both macro-CTAs in water while pendant drop measurements revealed higher interfacial tensions than A2 (1.2 and 3.5 mM m^{-1}) which is in line with the larger droplets formed (Fig. 2 & S3, S5, Tables S1–3†). In particular, we attribute the formation of these large nanodroplets to the hydrophilic nature of these macro-CTAs which reduces the surface-active property of these copolymers (Fig. 2, S3 & S5, Tables S1–3†). Another difference between A3/A4 with A0/A1/A2 macro-CTAs is that the former ones led to the formation of greyish solutions upon shaking while the latter ones spontaneously emulsified forming a white solution (Fig. 2e).

To ensure the validity of our conclusions, we also performed several additional experiments. It is noted that in all the aforementioned experiments we maintained a constant mass ratio of the macro-CTA, styrene, and SDS and hence the molar ratio of the copolymer to the other miniemulsion components was not constant as the copolymers possess different molecular weights. To address this, we also replicated our miniemulsions while keeping the molar ratio constant ([macro-CTA] : [STY] : [SDS] = 1 : 108 : 0.3 in 2 mL of deionized water, Fig. S6, and Table S4†). In another series of control experiments, we synthesized a new set of macro-CTAs in which a constant $M_n \sim 8000$ was maintained (macro-CTAs B0–B4) while keeping a similar DEGMA/HPMA ratio (0, 10, 18, 30, and 40% of HPMA respectively, Fig. 2f & S7, Table S5†). Pleasingly, very similar results were obtained for both control experiments highlighting that small variations in either the mass/molar ratio or molecular weight do not affect the formation of the miniemulsion (Fig. 2g & S8, 9, Table S5 and 6†). Importantly, and regardless of the HPMA composition, all macro-CTAs investigated are surface-active (interfacial tension <12 mM m^{-1}) as the surface tension of the bare styrene/water interface is about 32 mN m^{-1} (Fig. S10†). However, to form smaller nanodroplets, the amount of HPMA should be carefully regulated with the optimal composition found to be at approximately 20% (Fig. 2).

Low-energy miniemulsion RAFT polymerization with variable P(HPMA-*co*-DEGMA) composition

Considering that macro-CTAs A0, A1, and A2 can form stable miniemulsions both at room temperature and higher temperatures (70 °C), they would be ideal candidates to mediate a controlled RAFT miniemulsion polymerization (Fig. 2 & S3, Table S2†). To do so, a small amount of free radical initiator (*i.e.* AIBN) was also added before the formation of the miniemulsion without altering the stability of the nanodroplets ([macro-CTA] : [STY] : [AIBN] : [SDS] = 25 mg : 35 μL : 0.06 mg : 0.25 mg in 2 mL of deionized water).[37] It is highlighted that all polymerizations were performed in the absence of external deoxygenation by minimizing the headspace of the reaction vessel (Fig. 1).[44–48] It is also noted that the small induction

period observed at the early stage of the reaction is attributed to the oxygen consumption as under deoxygenated conditions, this induction period can be eliminated (Fig. S11, and Table S7†).[37] Importantly, all three macro-CTAs triggered a controlled RAFT polymerization resulting in the formation of well-defined block copolymers with narrow molar mass distributions ($Đ$ ~ 1.2–1.3, Fig. 3a, b & S12, Table S8†). We found that the polymerization rate was affected by the size of the initial nanodroplets: the smaller the size the faster the polymerization rate. In particular, macro-CTA A2 resulted in 96% of conversion within 6 h while A0 and A1 led to 48% and 65% of conversion respectively within the same time frame (Fig. 3b and Table S8†). Pleasingly, both A0 and A1 could also reach near-quantitative conversions (>94%) when the reactions were left to proceed for longer reactions times (Fig. S13, and Table S9†). The increased polymerization rate in smaller nanodroplets is related to the compartmentalization and segregation effects.[9] Instead, the RAFT polymerizations with macro-CTAs A3 and A4 were not successful leading to much higher dispersity values ($Đ$ ~ 1.6–2.4) accompanied by a shoulder attributed to conventional radical polymerization due to the absence of UV response (Fig. 3b & S12, Table S8†). This loss of control is due to unsuccessful conversion of all monomer droplets to nanodroplets when too hydrophilic macro-CTA A3 & A4 are utilized (Fig. 2 & S3, Table S2†). This result also supports our aforementioned findings that increasing the hydrophilicity of the copolymers leads to increasing their solubility in water, reducing their surface activity and producing more greyish/transparent solutions. The RAFT polymerizations were also conducted using a constant molar ratio ([macro-CTA] : [STY] : [AIBN] : [SDS] = 1 : 108 : 0.1 : 0.3, Fig. S14, and Table S10†). In a similar fashion to the previous experiments whereby the mass ratio was kept constant, macro-CTAs A3 and A4 also led to the uncontrolled polymerization of styrene. Instead, macro-CTAs A1 and A2 yielded the successful formation of block copolymers with relatively low dispersities ($Đ$

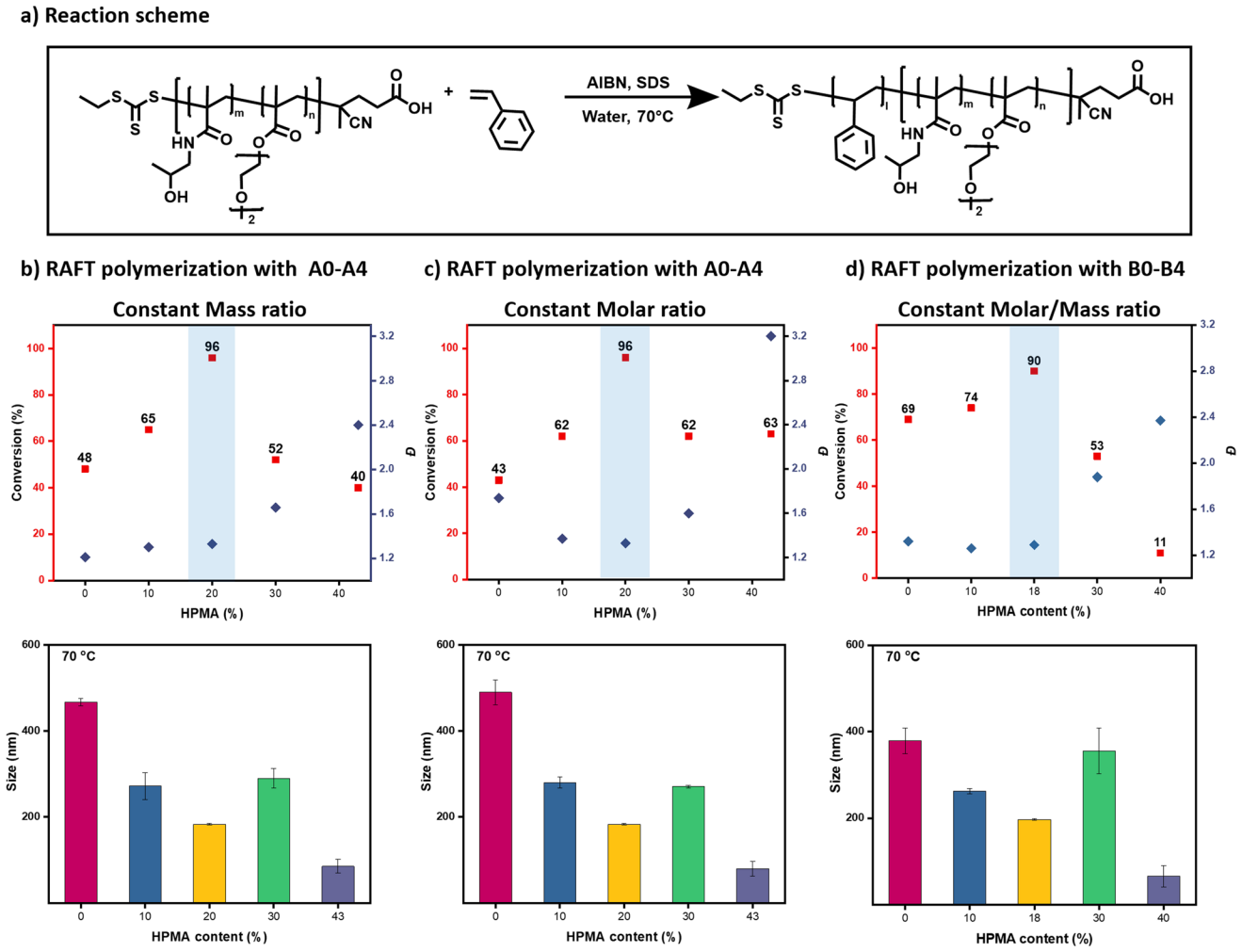

Fig. 3 (a) Scheme of RAFT miniemulsion polymerization of styrene. Conversion, dispersity and size (number by DLS) of miniemulsion formed (b) with A0–A4 while keeping the mass ratio constant ([macro-CTA] : [STY] : [AIBN] : [SDS] = 25 mg : 35 μL : 0.06 mg : 0.25 mg) or (c) the molar ratio constant ([macro-CTA] : [STY] : [AIBN] : [SDS] = 1 : 108 : 0.1 : 0.3), and formed (d) with B0–B4 keeping both mass/molar ratio constant ([macro-CTA] : [STY] : [AIBN] : [SDS] = 1 (25 mg) : 97 (35 μl) : 0.1 (0.07 mg) : 0.3 (0.25 mg)). All polymerization were performed in 2 mL of deionized water.

~ 1.3). However, when macro-CTA A0 was employed, much higher dispersities were obtained ($Đ$ ~ 1.7) (Fig. 3c & S14, Table S10†). The increase in dispersity is due to conventional radical polymerization and correlates to the lower mass content of macro-CTA used, which is not sufficient to be presented in all nanodroplets. It was thus concluded that for a successful RAFT polymerization, maintaining a sufficient amount of macro-CTA in the styrene phase is of paramount importance. We were also interested in conducting RAFT miniemulsion polymerizations with macro-CTAs B0-B4 in which the molecular weight of the macro-CTAs was kept constant. The results are summarized in Fig. 3d and follow a similar trend when compared to the experiments in which the mass ratio of the macro-CTAs A0–A4 was kept constant (Fig. 3d & S15, Table S11†).

The effect of molecular weight of P(HPMA-*co*-DEGMA) on low-energy miniemulsion formation and subsequent RAFT miniemulsion polymerization

Although we previously showed that the influence of small variations in the molecular weight of the macro-CTA was minor (compared to the effect of the ratio of DEGMA/HPMA), we sought to further explore the effect of molecular weight while keeping the percentage of HPMA constant. For example, one of the most efficient macro-CTAs both in terms of miniemulsion formation and controlled RAFT polymerization is A2 with M_n ~ 8900 ($Đ$ ~ 1.19, Fig. 2 & 3). Thus, we subsequently synthesized two additional macro-CTAs whereby the overall HPMA content was fixed at ~20%. Macro-CTA A5 was synthesized with a lower molecular weight than A2 (M_n ~ 5200, $Đ$ ~ 1.17) while macro-CTA A6 was prepared with a higher molecular weight (M_n ~ 17 100, $Đ$ ~ 1.17, Fig. 4 & S16, Table S12†). Pleasingly, all three macro-CTAs led to spontaneous emulsification and a white latex was formed within a few seconds of shaking ([macro-CTA] : [STY] : [SDS] = 25 mg : 35 μL : 0.25 mg in 2 mL of deonized water, Fig. S17†). Importantly, by analyzing the formed nanodroplets by DLS we observed that the size was within the miniemulsion range for all cases. However, the lowest molecular weight macro-CTA (A5) led to a much higher size (445 nm) while the highest molecular weight macro-CTA (A6) resulted in smaller nanodroplets (105 nm, Fig. 4a & S18, Table S13†). It also noted that 105 nm size is the smallest size we have been able to achieve utilizing this low-energy miniemulsion and no change in the size could be detected at higher temperatures (*i.e.* 70 °C, Fig. 4c and Table S13†) thus suggesting a stable miniemulsion. It can thus be concluded that by employing macro-CTAs with higher molecular weight, the particle size can be decreased further which is likely due to their increased surface-active property.

To rationalize these findings, we conducted interfacial tension measurements. The measurements showed that higher molecular weight macro-CTA (A6) displayed the lowest apparent interfacial tension (*i.e.* 0.12 mN m^{-1}) which is in line with the observed increased surface-active property (Fig. 4d and Table S12†). It is noted that the other two macro-CTAs are also surface-active albeit possessing slightly higher interfacial

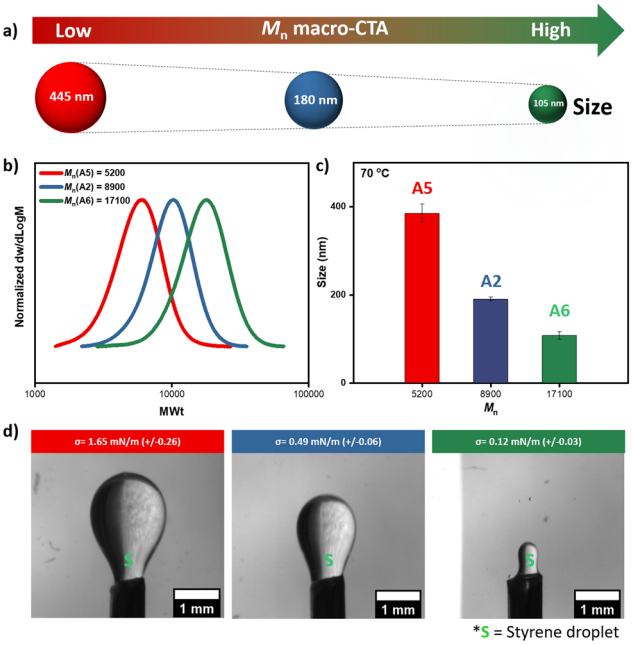

Fig. 4 (a) Schematic representation of the macro-CTA molecular weight influence on droplet sizes formed by low energy shaking of styrene at room temperature, (b) macro-CTAs A5, A2 and A6 SEC traces, (c) number mean by DLS at 70 °C of the low energy miniemulsion formed with macro-CTAs A5, A2 & A6 with the following formulation: [macro-CTA] : [STY] : [SDS] = 25 mg : 35 μL : 0.25 mg, in 2 mL of deonized water and (d) interfacial tension, by inverse pendant drop method, of a styrene droplet in aqueous solution of macro-CTAs A5, A2, and A6.

tension (Fig. 4d, Tables S1 & S12†). However, the difference in surface tension values of these macro-CTAs are not significant and within the measurement errors of the inverse pendant drop method, especially when the droplets appear to be wrinkled. We then assessed the ability of the three macro-CTAs to perform RAFT miniemulsion polymerizations. While A2 required approximately 6 h to reach near-quantitative conversion (*i.e.* 96%), A6 reached a similar conversion in under 4 h (*i.e.* 98%) thus further confirming that the smaller nanodroplets lead to a much faster polymerization rate (Fig. S19, and Table S14†). Instead, macro-CTA A5 led to a much slower miniemulsion RAFT polymerization with only 39% of conversion attained within 6 h. However, increasing monomer conversion was possible by increasing the reaction time (Fig. S19 and Table S14†). Pleasingly, in all cases, well-defined block copolymers could be synthesized with narrow molar mass distributions ($Đ$ ~ 1.2–1.3, Fig. S19, and Table S14†).

Low-energy miniemulsion utilizing various surface-active random copolymers

Our data have shown that the role of DEGMA is very important to the formation of the low-energy miniemulsion as even in the absence of HPMA, PDEGMA homopolymer can still form stable miniemulsions exhibiting low interfacial tension (Fig. 2). Instead, the role of HPMA is to enhance the hydrophilicity of the macro-CTA and reduce the nanodroplet size

by further lowering the interfacial tension (Fig. 2). It is also noted that PHPMA homopolymer cannot form a miniemulsion due to its highly hydrophilic nature. At the same time, HPMA is a relatively costly monomer which encouraged us to investigate less inexpensive alternatives and expand the availability of surface-active agents for low-energy miniemulsion and RAFT polymerization. Triethylene glycol methyl ether methacrylate (TEGMA) and poly(ethylene glycol) methyl ether methacrylate (PEGMA) were first selected as hydrophilic alternatives and their content was fixed at approximately ~20%. The two macro-CTAs, C0 and D0, were successfully synthesized yielding polymers with low dispersity ($Đ$ < 1.2, Fig. 5a & S20a, b, S21, 22, Table S15†). However, both macro-CTAs led to the formation of large nanodroplets (~500 nm) and higher interfacial tension (Fig. 5b, c, Tables S15 and 16†). In particular, while the bare PDEGMA exhibits an interfacial tension of 11.72 mN m^{-1}, the addition of either TEGMA or PEGMA did not lead to a significant decrease of the initial value (>9.2 mN m^{-1} in both cases, Fig. 2 & 5, Tables S1 & S15†). This is in contrast to P(HPMA-*co*-DEGMA) which resulted in a much lower interfacial tension (~0.49 mN m^{-1}, Fig. 2, Table S1†).

To better mimic the chemical structure of HPMA, we subsequently incorporated hydroxyethyl methacrylate (HEMA) within the macro-CTA composition (E0, Fig. 5a, S20c & S23, Table S15†). Pleasingly, the nanodroplet size was decreased to ~300 nm and this can be explained by the lower interfacial tension obtained (2.6 mN m^{-1}, Fig. 5b, c, Tables S15 and 16†). Encouraged by this finding, we also chose methacrylamide (MAAm) as another potential alternative (F0, Fig. 5a, S20d & S24, Table S15†). Notably, when P(MAAm-*co*-DEGMA) was employed, the nanodroplet size could be further decreased to 144 nm and this was accompanied by an even lower interfacial tension of the macro-CTA (0.18 mN m^{-1}, Fig. 5b, c, Tables S15 and 16†). It should also be highlighted that all employed macro-CTAs were surface active although only P(HEMA-*co*-DEGMA) and P(MAAm-*co*-DEGMA) further reduced the interfacial tension to a lower value than the homopolymer PDEGMA (Fig. 2, 5 & S10†). It is noted that the key to reduce the interfacial tension is the presence of the copolymers on the nanodroplet surface. While TEGMA and PEGMA could increase the hydrophilicity of their copolymers (the T_{cp}s increase from 24 °C to 28 °C and 34 °C, respectively), they still partition very well in the styrene phase, as shown in our extrac-

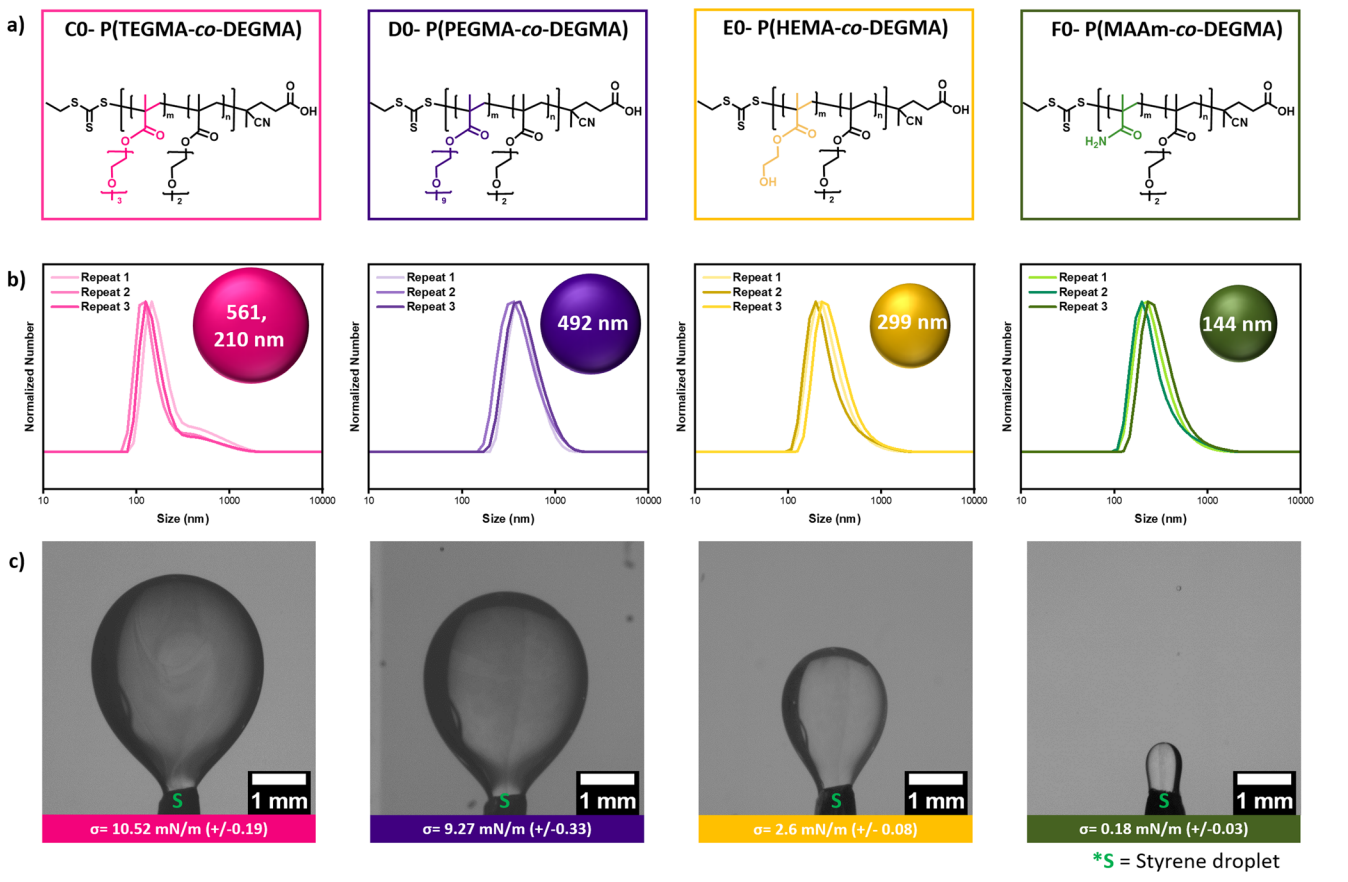

Fig. 5 (a) Chemical structure of macro-CTAs, poly(TEGMA-*co*-DEGMA) (C0), poly(PEGMA-*co*-DEGMA) (D0), poly(HEMA-*co*-DEGMA) (E0) and poly(MAAm-*co*-DEGMA) (F0), (b) number mean size by DLS with the following formulation: [macro-CTA] : [STY] : [SDS] = 25 mg : 35 μL : 0.25 mg, in 2 mL of deionized water (three repeats, 25 °C), (c) interfacial tension, by inverse pendant drop method, of a styrene droplet in aqueous solution of macro-CTAs C0, D0, E0 and F0.

tion experiments (Fig. S24†), probably due to the similar chemical composition to DEGMA (*i.e.*, the ethylene glycol repeating units). The hydrophilicity of P(HEMA-*co*-DEGMA) and P(MAAm-*co*-DEGMA) copolymers is not higher than P(PEGMA-*co*-DEGMA), but the presence of a hydroxy or amide group reduces their partition in the styrene phase and increase their surface-active property, as evident by the lower interfacial tension and the smaller nanodroplet size (Fig. 5, Tables S15 and 16†). This result suggests that in addition to increasing the copolymer hydrophilicity by incorporating more HPMA, reducing the solubility of the copolymer in the styrene phase is another way to improve the surface activity of the statistical copolymers.

Shape-controlled nanoparticles utilizing P(MAAm-*co*-DEGMA)

Since the incorporation of MAAm resulted in the lowest interfacial tension and the smaller nanodroplet size, we further investigated this system by both lowering and increasing the MAAm content (Fig. S26, 27 and Table S17†). In particular, by lowering the MAAm content from 23% to 14%, the nanodroplet size and interfacial tension were increased to 354 nm and σ = 1.43 mN m^{-1} respectively. In contrast, increasing the MAAm content to 35% led to a lack of emulsification and bimodal particles sizes which was attributed to the high hydrophilicity of this macro-CTA (Fig. 6a–c, Tables S17 and 18†). This result is consistent with our data in which we changed the amount of HPMA (Fig. 2). The initial P(MAAm-*co*-DEGMA), F0, with 23% of MAAm content was subsequently employed to perform RAFT polymerization ([macro-CTA] : [STY] : [AIBN] : [SDS] = 25 mg : 35 μL : 0.06 mg : 0.25 mg in 2 mL of deionized water). Within 7 h, a near-quantitative conversion could be obtained (*i.e.* 98%) while the final P(MAAm-*co*-DEGMA)-*b*-PS displayed a controlled molecular weight and narrow molar mass distributions ($Đ \sim 1.22$, Fig. 6d and Table S19†).

We were then interested in controlling the shape of the resulting nanoparticles through our recently developed transformer-induced metamorphosis (TIM) method.[49] This method operates at room temperature by adding a small amount of a molecular transformer (*i.e.* toluene) that resembles the solubility of the core and allows for the transformation of the nano-

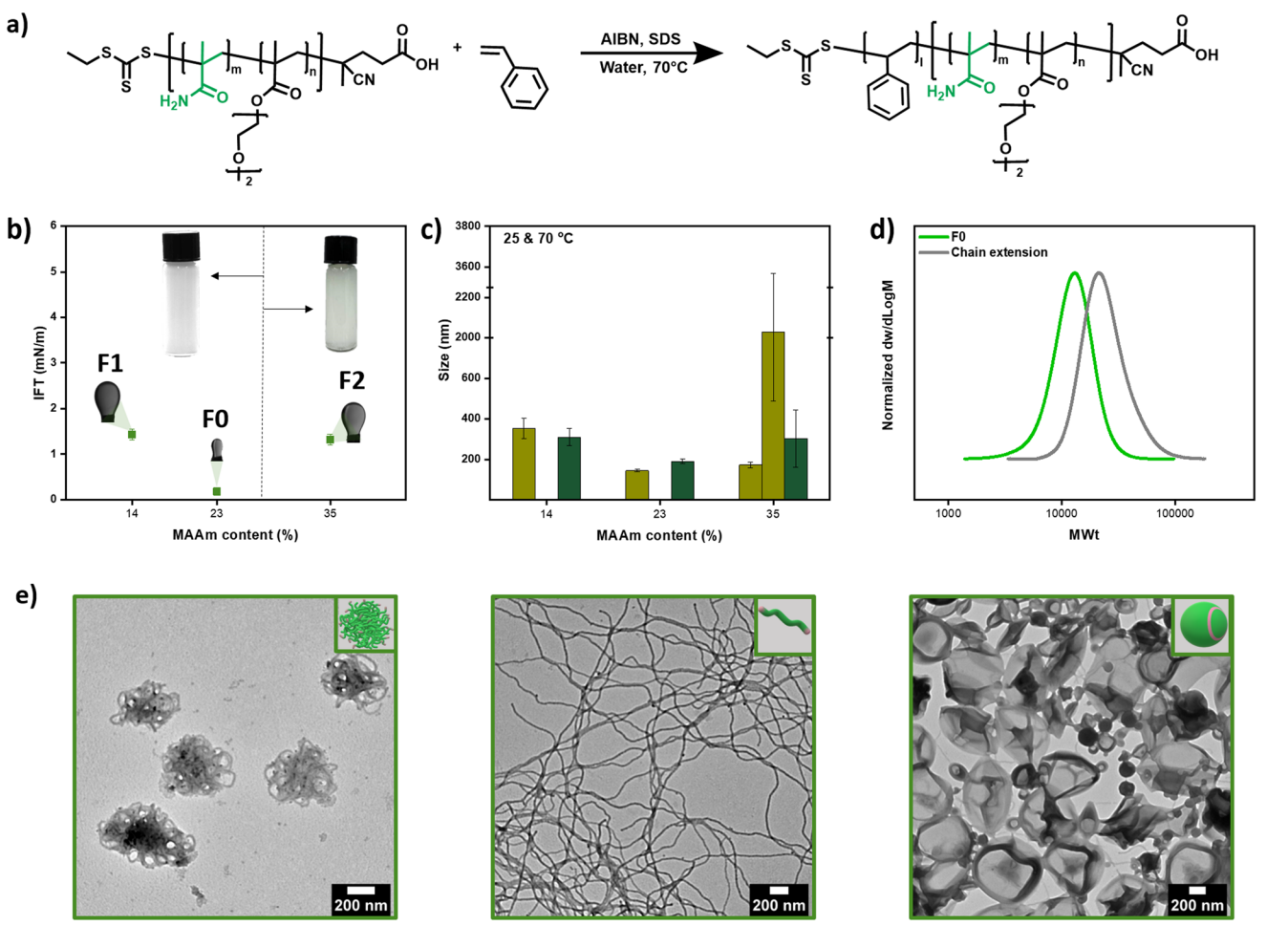

Fig. 6 (a) Scheme of RAFT miniemulsion polymerization of styrene using P(MAAm-*co*-DEGMA) as macro-CTA, (b) interfacial tension by inverse pendant drop method of a styrene droplet in aqueous solution of macro-CTAs F1, F0 and F2 and pictures of the (mini)emulsions, (c) number mean size by DLS of the resulting miniemulsion at 25 °C (light greeen) and 70 °C (dark green), (d) RAFT miniemulsion polymerization of styrene using F0 as macro-CTA and (e) morphologies (worms balls M_n = 13 200, worms M_n = 14 000, and vesicles M_n = 19 700, Table S20†).

particles to a higher ordered morphology. Specifically, by changing the molecular weight of the second block while altering the amount of added transformer (*i.e.* toluene), different nanoparticle shapes could be obtained ranging from spheres, worm balls to worms and vesicles (M_n = 13 200, 14 000, 19 700, Fig. 6e, Fig. S28 and Table S20†). Importantly, all acquired morphologies were of high purity, as observed by transmission electron microscopy (TEM), and the data are presented in Fig. 6e.

Conclusions

In summary, we have elucidated the structure/property relationship of surface-active statistical copolymers used for low-energy miniemulsion and RAFT polymerization and applied the acquired knowledge to design new copolymers. All these copolymers were surface-active and able to decrease the interfacial tension between water and styrene. We first used P(HPMA-*co*-DEGMA) as a model statistical copolymer and found that both the percentage of HPMA as well as the molecular weight of the macro-CTA affect the size of the obtained nanodroplets as well as the rate of polymerization. This was attributed to the change in the interfacial tension whereby a lower interfacial tension value led to the formation of nanodroplets of smaller size. To further expand the scope of our method we then sought to replace HPMA with more inexpensive alternatives. We found that when both HEMA and MAAm were incorporated within the statistical copolymer composition, rapid emulsification took place while their corresponding macro-CTAs displayed very low interfacial tension values (<2.6 mN m^{-1}). As P(MAAm-*co*-DEGMA) presented the lowest interfacial tension (0.18 mN m^{-1}) and led to the formation of the smallest nanodroplets (~144 nm) we subsequently employed this macro-CTA to trigger the controlled RAFT miniemulsion polymerization of styrene. Last but not least, by applying our recently developed transformer-induced metamorphosis strategy we were able to control the shape of the polymeric nanoparticles acquiring worm-balls, worms, and vesicles at high purity. Our work provides useful guidelines for the design of surface-active copolymers, expanding the availability of surface-active agents required in low-energy miniemulsion and RAFT miniemulsion polymerization.

Author contributions

Manon Rolland: conceptualization, investigation, analysis, data curation, methodology, visualization, writing-original draft. Eric R. Dufresne: methodology, software, writing – review & editing. Nghia P. Truong: conceptualization, investigation, analysis, methodology, project administration, supervision, writing – review & editing, Athina Anastasaki: conceptualization, investigation, funding, analysis, methodology, project administration, resources, supervision, writing – review & editing.

Conflicts of interest

There are no conflicts to declare.

Acknowledgements

A. A gratefully acknowledges ETH Zurich for financial support. N. P. T. acknowledges the award of a DECRA Fellowship and DP from the ARC (DE180100076 and DP200100231). We are grateful to ScopeM (ETH Zurich) for access to the electron microscopy facilities. Ms. Maria-Nefeli Antonopoulou is acknowledged for her support with NMR measurements during the revisions.

References

1 J. M. Asua, *Prog. Polym. Sci.*, 2002, **27**, 1283–1346.
2 A. Maali and M. H. Mosavian, *J. Dispersion Sci. Technol.*, 2013, **34**, 92–105.
3 J. Qiu, B. Charleux and K. Matyjaszewski, *Prog. Polym. Sci.*, 2001, **26**, 2083–2134.
4 T. J. Ashaolu, *Environ. Chem. Lett.*, 2021, **19**, 3381–3395.
5 Y. Singh, J. G. Meher, K. Raval, F. A. Khan, M. Chaurasia, N. K. Jain and M. K. Chourasia, *J. Controlled Release*, 2017, **252**, 28–49.
6 P. Sanguansri and M. A. Augustin, *Trends Food Sci. Technol.*, 2006, **17**, 547–556.
7 K. Parkatzidis, H. S. Wang, N. P. Truong and A. Anastasaki, *Chem*, 2020, **6**, 1575–1588.
8 G. K. Clothier, T. R. Guimarães, G. Moad and P. B. Zetterlund, *Macromolecules*, 2022, **6**, 1981–1991.
9 P. B. Zetterlund, *Polym. Chem.*, 2011, **2**, 534–549.
10 Y. Wang, S. Dadashi-Silab and K. Matyjaszewski, *ACS Macro Lett.*, 2018, **7**, 720–725.
11 K. Jung, J. Xu, P. B. Zetterlund and C. Boyer, *ACS Macro Lett.*, 2015, **4**, 1139–1143.
12 S.-P. Wen, Q. Yue and L. A. Fielding, *Polym. Chem.*, 2021, **12**, 2122–2131.
13 P. B. Zetterlund, Y. Kagawa and M. Okubo, *Chem. Rev.*, 2008, **108**, 3747–3794.
14 K. Landfester, N. Bechthold, S. Förster and M. Antonietti, *Macromol. Rapid Commun.*, 1999, **20**, 81–84.
15 J. Ugelstad, M. El-Aasser and J. Vanderhoff, *J. Polym. Sci., Part B: Polym. Lett.*, 1973, **11**, 503–513.
16 J. K. Oh, *J. Polym. Sci., Part A: Polym. Chem.*, 2008, **46**, 6983–7001.
17 P. B. Zetterlund, S. C. Thickett, S. Perrier, E. Bourgeat-Lami and M. Lansalot, *Chem. Rev.*, 2015, **115**, 9745–9800.
18 N. Anton, J.-P. Benoit and P. Saulnier, *J. Controlled Release*, 2008, **128**, 185–199.
19 J. M. Asua, *Prog. Polym. Sci.*, 2014, **39**, 1797–1826.
20 D. J. McClements and J. Rao, *Crit. Rev. Food Sci. Nutr.*, 2011, **51**, 285–330.

21 T. Boursier, I. Chaduc, J. Rieger, F. d'Agosto, M. Lansalot and B. Charleux, *Polym. Chem.*, 2011, **2**, 355–362.
22 Y. Wang, L. Fu and K. Matyjaszewski, *ACS Macro Lett.*, 2018, **7**, 1317–1321.
23 J. Feng, C. Rodríguez-Abreu, J. Esquena and C. Solans, *J. Surfactants Deterg.*, 2020, **23**, 677–685.
24 J. C. López-Montilla, P. E. Herrera-Morales, S. Pandey and D. O. Shah, *J. Dispersion Sci. Technol.*, 2002, **23**, 219–268.
25 J. Galindo-Alvarez, D. Boyd, P. Marchal, C. Tribet, P. Perrin, E. Marie-Bégué, A. Durand and V. Sadtler, *Colloids Surf., A*, 2011, **374**, 134–141.
26 N. Nauman, N. Zaquen, T. Junkers, C. Boyer and P. B. Zetterlund, *Macromolecules*, 2019, **52**, 4492–4499.
27 U. El-Jaby, M. Cunningham and T. F. McKenna, *Macromol. Rapid Commun.*, 2010, **31**, 558–562.
28 N. Nauman, C. Boyer and P. B. Zetterlund, *Colloid Polym. Sci.*, 2021, 1–9.
29 J. Feng, M. Roché, D. Vigolo, L. N. Arnaudov, S. D. Stoyanov, T. D. Gurkov, G. G. Tsutsumanova and H. A. Stone, *Nat. Phys.*, 2014, **10**, 606–612.
30 I. Solè, C. Solans, A. Maestro, C. González and J. Gutiérrez, *J. Colloid Interface Sci.*, 2012, **376**, 133–139.
31 N. P. Truong, G. R. Jones, K. G. Bradford, D. Konkolewicz and A. Anastasaki, *Nat. Rev. Chem.*, 2021, **5**, 859–869.
32 S. M. Hashemnejad, A. Z. M. Badruddoza, B. Zarket, C. R. Castaneda and P. S. Doyle, *Nat. Commun.*, 2019, **10**, 2749.
33 C. Solans and I. Solé, *Curr. Opin. Colloid Interface Sci.*, 2012, **17**, 246–254.
34 S. Cheng, Y. Guo and P. B. Zetterlund, *Macromolecules*, 2010, **43**, 7905–7907.
35 Y. Guo, J. Liu and P. B. Zetterlund, *Macromolecules*, 2010, **43**, 5914–5916.
36 S. Cheng, S. S. Ting, F. P. Lucien and P. Zetterlund, *Macromolecules*, 2012, **45**, 1803–1810.
37 M. Rolland, N. P. Truong, K. Parkatzidis, E. H. Pilkington, A. L. Torzynski, R. W. Style, E. R. Dufresne and A. Anastasaki, *JACS Au*, 2021, **1**, 1975–1986.
38 N. P. Truong, J. F. Quinn, A. Anastasaki, D. M. Haddleton, M. R. Whittaker and T. P. Davis, *Chem. Commun.*, 2016, **52**, 4497–4500.
39 M. Ijavi, R. W. Style, L. Emmanouilidis, A. Kumar, S. M. Meier, A. L. Torzynski, F. H. Allain, Y. Barral, M. O. Steinmetz and E. R. Dufresne, *Soft Matter*, 2021, **17**, 1655–1662.
40 J. Israelachvili, *Colloids Surf., A*, 1994, **91**, 1–8.
41 J. N. Israelachvili, *Intermolecular and surface forces*, Academic press, 2011.
42 W. C. Griffin, *J. Soc. Cosmet. Chem.*, 1949, **1**, 311–326.
43 F. Ravera, M. Ferrari and L. Liggieri, *Adv. Colloid Interface Sci.*, 2000, **88**, 129–177.
44 E. Liarou, R. Whitfield, A. Anastasaki, N. G. Engelis, G. R. Jones, K. Velonia and D. M. Haddleton, *Angew. Chem., Int. Ed.*, 2018, **57**, 8998–9002.
45 A. Theodorou, E. Liarou, D. M. Haddleton, I. G. Stavrakaki, P. Skordalidis, R. Whitfield, A. Anastasaki and K. Velonia, *Nat. Commun.*, 2020, **11**, 1486.
46 J. Yeow, R. Chapman, A. J. Gormley and C. Boyer, *Chem. Soc. Rev.*, 2018, **47**, 4357–4387.
47 G. Szczepaniak, L. Fu, H. Jafari, K. Kapil and K. Matyjaszewski, *Acc. Chem. Res.*, 2021, **54**, 1779–1790.
48 M. Rolland, R. Whitfield, D. Messmer, K. Parkatzidis, N. P. Truong and A. Anastasaki, *ACS Macro Lett.*, 2019, **8**, 1546–1551.
49 K. Parkatzidis, N. P. Truong, M. Rolland, V. Lutz-Bueno, E. H. Pilkington, R. Mezzenga and A. Anastasaki, *Angew. Chem., Int. Ed.*, 2022, e202113424.